Itinerant in-plane magnetic fluctuations and many-body correlations in Na$_x$CoO$_2$

M. M. Korshunov,[1,2,*] I. Eremin,[2,3] A. Shorikov,[4] V. I. Anisimov,[4] M. Renner,[3] and W. Brenig[3]

[1]*L. V. Kirensky Institute of Physics, Siberian Branch of Russian Academy of Sciences, 660036 Krasnoyarsk, Russia*
[2]*Max-Planck-Institut für Physik Komplexer Systeme, D-01187 Dresden, Germany*
[3]*Institute für Mathematische und Theoretische Physik, TU Braunschweig, 38106 Braunschweig, Germany*
[4]*Institute of Metal Physics, Russian Academy of Sciences-Ural Division, 620041 Yekaterinburg GSP-170, Russia*

Based on the *ab initio* band structure for Na$_x$CoO$_2$, we derive the single-electron energies and the effective tight-binding description for the t_{2g} bands using projection procedure. Due to the presence of the next-nearest-neighbor hoppings, a local minimum in the electronic dispersion close to the Γ point of the first Brillouin zone forms. Correspondingly, in addition to a large Fermi surface, an electron pocket close to the Γ point emerges at high doping concentrations. The latter yields a scattering channel, resulting in a peak structure of the itinerant magnetic susceptibility at small momenta. This indicates dominant itinerant in-plane ferromagnetic fluctuations above a certain critical concentration x_m, in agreement with neutron scattering data. Below x_m, the magnetic susceptibility shows a tendency toward the antiferromagnetic fluctuations. We further analyze the many-body effects on the electronic and magnetic excitations using various approximations applicable for different U/t ratios.

PACS number(s): 74.70.−b, 31.15.Ar, 71.10.−w, 75.40.Cx

I. INTRODUCTION

The recent discovery of the superconductivity in hydrated lamellar cobaltate Na$_x$CoO$_2$·yH$_2$O (Ref. 1) has raised tremendous interest in the nature and symmetry of the superconductive pairing in these materials. The phase diagram of this compound, with varying electron doping concentration x and water intercalation y, is rich and complicated; in addition to superconductivity, it exhibits magnetic and charge orders, and some other structural transitions.[2–5] The parent compound, Na$_x$CoO$_2$, is a quasi-two-dimensional system with Co in CoO$_2$ layers forming a triangular lattice where the Co-Co in-plane distance is two times smaller than the interplane one. Na ions reside between the CoO$_2$ layers and donate additional x electrons to the layer, lowering the Co valence from Co^{4+} (3d^5 configuration) to Co^{3+} (3d^6 configuration) upon changing x from 0 (CoO$_2$) to 1 (NaCoO$_2$). The hole in the d orbital occupies one of the t_{2g} levels, which are lower than e_g levels by about 2 eV.[6] The degeneracy of the t_{2g} levels is partially lifted by the trigonal crystal-field distortion, which splits the former into the higher-lying a_{1g} singlet and the lower two e'_g states.

First-principles local-density approximation (LDA) and local density approximation+Hubbard U (LDA+U) band structure calculations predict Na$_x$CoO$_2$ to have a large Fermi surface (FS) centered around the $\Gamma=(0,0,0)$ point with mainly a_{1g} character and six hole pockets near the K $=(0,4\pi/3,0)$ points of the hexagonal Brillouin zone of mostly e'_g character for a wide range of x.[6,7] At the same time, recent surface-sensitive angle-resolved photoemission spectroscopy (ARPES) experiments[8–11] reveal a doping-dependent evolution of the Fermi surface, which shows no sign of hole pockets for a wide range of Na concentrations, i.e., $(0.3 \leqslant x \leqslant 0.8)$. Instead, the Fermi surface is observed to be centered around the Γ point and to have mostly a_{1g} character. Furthermore, a dispersion of the valence band is measured which is only half of that calculated within the LDA.

This indicates the importance of the electronic correlations in Na$_x$CoO$_2$.

Shubnikov–de Haas effect measurements revealed two well-defined frequencies in Na$_{0.3}$CoO$_2$, suggesting either the existence of Na superstructures or the presence of the e'_g pockets.[12] The latter possibility was found to be incompatible with existing specific heat data. Also, within the LDA scheme, the Na disorder was shown to destroy the small e'_g pockets in Na$_{2/3}$CoO$_2$ because of their tendency toward localization.[13]

The hole pockets are absent in the local spin density approximation+U (LSDA+U) calculations.[14] However, in this approach, the insulating gap is formed by a splitting of the local single-electron states due to spin-polarization, resulting in a spin polarized Fermi surface with an area twice as large as that observed through ARPES.

The dynamical character of the strong electron correlations has been taken into account within dynamical mean-field theory (DMFT) calculations[15] and, surprisingly, has led to an enhancement of the area of the small Fermi surface pockets, in contrast to the experimental observations. At the same time, the use of the strong-coupling Gutzwiller approximation within the multiorbital Hubbard model with fitting parameters[16] yields an absence of the hole pockets at the Fermi surface. According to these findings, the bands crossing the Fermi surface have a_{1g} character.

Concerning the magnetic properties, LSDA predicts Na$_x$CoO$_2$ to have a weak intraplane itinerant ferromagnetic (FM) state for nearly all Na concentrations, $0.3 \leqslant x \leqslant 0.7$.[17] On the contrary, neutron scattering finds on A-type antiferromagnetic order at $T_m \approx 22$ K with an inter(intra)plane exchange constant $J_{c(ab)}=12(-6)$ meV and with ferromagnetic ordering within Co layer *only* for $0.75 \leqslant x \leqslant 0.9$.[18–20]

In this paper, we derive an effective low-energy model describing the bands crossing the Fermi level on the basis of the LDA band-structure calculations. Due to the FS topology inferred from LDA band structure, the magnetic susceptibil-

ity $\chi_0(\mathbf{q}, \omega=0)$ reveals two different regimes. For $x<0.56$, the susceptibility shows pronounced peaks at the antiferromagnetic (AFM) wave vector $\mathbf{Q}_{AFM}$ $=\{(2\pi/3, 2\pi/\sqrt{3}), (4\pi/3, 0)\}$, resulting in a tendency toward in-plane 120° AFM order. For $x>0.56$, the susceptibility is peaked at small momenta near $\mathbf{Q}_{FM}=(0,0)$. This clearly demonstrates the tendency of the system toward an itinerant in-plane FM state. We find that the formation of the electron pocket around the Γ point is crucial to the in-plane FM ordering at high doping concentrations. We further analyze the role of the many-body effects calculated within the fluctuation-exchange (FLEX), Gutzwiller, and Hubbard-I approximations.

The paper is organized as follows. In Sec. II, the LDA band-structure and tight-binding model parameters derivation are described. The doping-dependent evolution of the magnetic susceptibility within the tight-binding model is presented in Sec. III. The role of strong electron correlations is analyzed in Sec. IV. The last section summarizes our study.

II. TIGHT-BINDING MODEL

The band structure of Na$_{0.61}$CoO$_2$ was obtained within the LDA (Ref. [21]) in the framework of the tight-binding approach to the linear muffin-tin-orbitals using atomic sphere approximation (TB-LMTO-ASA)[22] computation scheme. This compound crystallizes at 12 K in the hexagonal structure ($P6_3/mmc$ symmetry group) with $a=2.831\,76$ Å and $c=10.843\,12$ Å.[23] A displacement of Na atoms from their ideal sites $2d$ $(1/3, 2/3, 3/4)$ on about 0.2 Å is observed in defected cobaltates for both room and low temperatures. This is probably due to the repulsion of the randomly distributed Na atoms, locally violating hexagonal symmetry.[23] In this study, Na atoms were shifted back to the high-symmetry $2d$ sites. Oxygen was situated in the high-symmetry $4f$ position $(1/3, 2/3, 0.09057(7))$. The obtained Co-O distance is 1.9066 Å, which agrees well with the experimentally observed distance, 1.9072(4) Å.[23] This unit cell was used for all doping concentrations. The effect of the doping was taken into account within the virtual crystal approximation where each Co site has six nearest-neighbor virtual atoms with a fractional number of valence electrons x and a core charge $10+x$ instead of randomly located Na. Note that all core states of the virtual atom are left unchanged and correspond to Na ones. We have chosen $4s$, $4p$, and $3d$ states of Co, $2s$, $2p$, and $3d$ states of O, and $3s$, $3p$, and $3d$ states of Na as the valence states for the TB-LMTO-ASA computation scheme. The radii of atomic spheres are 1.99 a.u. for Co, 1.61 a.u. for O, and 2.68 a.u. for Na. Two classes of empty spheres (pseudoatoms without core states) were added in order to fill the unit cell volume.

In order to find an appropriate basis, the occupation matrix was diagonalized and its eigenfunctions were used as the new local orbitals. This procedure takes into account the real distortion of the crystal structure. The new orbitals are not pure trigonal a_{1g} and e_g' orbitals but we still use the former notations for the sake of simplicity. 288 k points in the whole Brillouin zone were used for the band-structure calculations ($12\times12\times2$ mesh for k_x, k_y, and k_z, respectively).
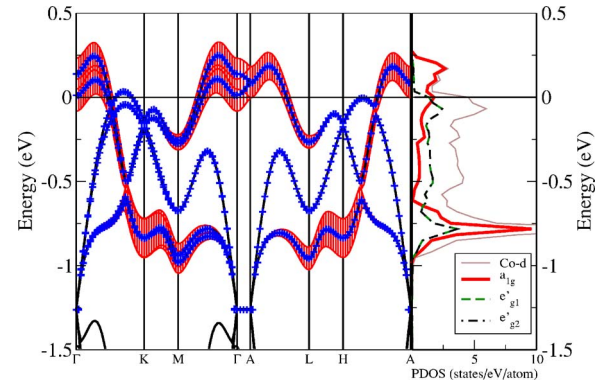

FIG. 1. (Color online) Calculated near-Fermi-level LDA band structure and partial density of states (PDOS) for Na$_{0.33}$CoO$_2$. The contribution of Co-a_{1g} states is denoted by the vertical broadening (in red) of the bands with thickness proportional to the weight of the contribution. The crosses indicate the dispersion of the bands obtained by projection on the t_{2g} orbitals. The horizontal line at zero energy denotes the Fermi level.

The bands crossing the Fermi level are shown in Fig. 1. One sees that they have mostly a_{1g} character, consistent with previous LDA findings.[6] Note that the small FS pockets near the K point with e_g' symmetry present at $x=0.33$ [see Fig. 2(b)] disappear at higher doping concentrations because the corresponding bands sink below the Fermi level. The difference in the dispersion along the K-M and L-H directions is due to a non-negligible interaction between CoO$_2$ planes. A small gap between Co $3d$ and O $2p$ states at about -1.25 eV present for $x=0.61$ disappears for $x=0.33$ due to the shift of the d band to lower energy upon decreasing the number of electrons.

In the following, we restrict ourselves to the model with the in-plane hoppings inside the CoO$_2$ layer to describe the doping dependence of the itinerant in-plane magnetic order. Hence, we neglect the bonding-antibonding (bilayer) splitting present in the LDA bands. This assumption seems to be justified since the largest interlayer hopping matrix element is an order of magnitude smaller than the intraplane one (0.012 vs 0.12 eV).

To construct the effective Hamiltonian and to derive the effective Co-Co hopping integrals $t_{fg}^{\alpha\beta}$ for the t_{2g} manifold, we apply the projection procedure.[24,25] Here, $\alpha\beta$ denotes a
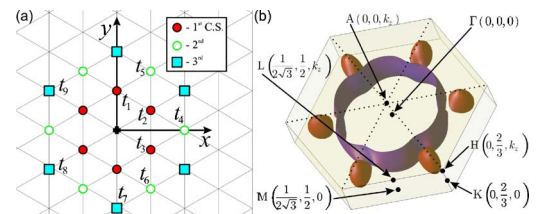

FIG. 2. (Color online) (a) Schematic crystal structure of the Co layer in Na$_x$CoO$_2$ with hopping notations within the first three co-ordination spheres (CS). (b) LDA-calculated Fermi surface with cylindrical part (violet) having mostly a_{1g} character and six hole pockets (red) having mostly e_g' character. k_x and k_y coordinates of the symmetry points are given in units of $2\pi/a$ with a being the in-plane lattice constant.

TABLE I. Single-electron energies ε^α (relative to $\varepsilon^{a_{1g}}$) and in-plane hopping integrals $t_n^{\alpha\beta}$ for Na$_x$CoO$_2$, where $x=0.33$, 0.61, and 0.7 (all values are in eV).

		In-plane vector	$(0, 1)$	$(\frac{\sqrt{3}}{2}, \frac{1}{2})$	$(\frac{\sqrt{3}}{2}, -\frac{1}{2})$	$(\sqrt{3}, 0)$	$(\frac{\sqrt{3}}{2}, \frac{3}{2})$	$(\frac{\sqrt{3}}{2}, -\frac{3}{2})$	$(0, 2)$	$(\sqrt{3}, 1)$	$(\sqrt{3}, -1)$
α	ε^α	$\alpha \rightarrow \beta$	$t_1^{\alpha\beta}$	$t_2^{\alpha\beta}$	$t_3^{\alpha\beta}$	$t_4^{\alpha\beta}$	$t_5^{\alpha\beta}$	$t_6^{\alpha\beta}$	$t_7^{\alpha\beta}$	$t_8^{\alpha\beta}$	$t_9^{\alpha\beta}$
						$x=0.33$					
a_{1g}	0.000	$a_{1g} \rightarrow a_{1g}$	0.123	0.123	0.123	−0.022	−0.022	−0.021	−0.025	−0.025	−0.025
		$a_{1g} \rightarrow e'_{g1}$	−0.044	0.089	−0.044	0.010	0.010	−0.021	−0.021	0.042	−0.021
e'_{g1}	−0.053	$a_{1g} \rightarrow e'_{g2}$	−0.077	0.000	0.077	0.018	−0.018	0.000	−0.036	0.000	0.036
		$e'_{g1} \rightarrow e'_{g1}$	−0.069	−0.005	−0.069	0.018	0.018	−0.026	−0.017	−0.085	−0.017
e'_{g2}	−0.053	$e'_{g1} \rightarrow e'_{g2}$	0.037	0.000	−0.037	−0.026	0.026	0.000	−0.039	0.000	0.039
		$e'_{g2} \rightarrow e'_{g2}$	−0.026	−0.090	−0.027	−0.011	−0.011	0.033	−0.062	0.006	−0.062
						$x=0.61$					
a_{1g}	0.000	$a_{1g} \rightarrow a_{1g}$	0.110	0.110	0.110	−0.019	−0.019	−0.019	−0.023	−0.023	−0.023
		$a_{1g} \rightarrow e'_{g1}$	−0.050	0.100	−0.050	0.008	0.008	−0.016	−0.017	0.035	−0.017
e'_{g1}	−0.028	$a_{1g} \rightarrow e'_{g2}$	0.087	0.000	−0.087	−0.014	0.014	0.000	0.030	−0.000	−0.030
		$e'_{g1} \rightarrow e'_{g1}$	−0.069	−0.031	−0.069	0.015	0.015	−0.022	−0.016	−0.076	−0.016
e'_{g2}	−0.028	$e'_{g1} \rightarrow e'_{g2}$	−0.022	0.000	0.022	0.021	−0.021	0.000	0.035	0.000	−0.035
		$e'_{g2} \rightarrow e'_{g2}$	−0.044	−0.081	−0.044	−0.009	−0.009	0.027	−0.056	0.005	−0.056
						$x=0.7$					
a_{1g}	0.000	$a_{1g} \rightarrow a_{1g}$	0.105	0.105	0.105	−0.018	−0.018	−0.018	−0.022	−0.022	−0.022
		$a_{1g} \rightarrow e'_{g1}$	−0.052	0.104	−0.052	0.007	0.007	−0.015	−0.016	0.033	−0.016
e'_{g1}	−0.019	$a_{1g} \rightarrow e'_{g2}$	−0.090	0.000	−0.090	0.013	−0.013	0.000	−0.028	0.000	0.028
		$e'_{g1} \rightarrow e'_{g1}$	−0.068	−0.039	−0.068	0.014	0.014	−0.020	−0.015	−0.073	−0.015
e'_{g2}	−0.019	$e'_{g1} \rightarrow e'_{g2}$	0.016	0.000	−0.016	−0.020	0.020	0.000	−0.034	0.000	0.034
		$e'_{g2} \rightarrow e'_{g2}$	−0.048	−0.077	−0.049	−0.009	−0.009	0.026	−0.054	0.005	−0.054

pair of orbitals, a_{1g}, e'_{g1}, or e'_{g2}. The indices f and g correspond to the Co sites on the triangular lattice. The obtained hoppings and the single-electron energies are given in Table I for three different doping concentrations. A comparison between the bands obtained using the projection procedure and those obtained through the LDA bands is shown in Fig. 1, confirming the Co-t_{2g} nature of the near-Fermi level bands.[6,26] For simplicity, we have enumerated site pairs with $n=0,1,2,\ldots$, $t_{fg}^{\alpha\beta} \rightarrow t_n^{\alpha\beta}$ [see Fig. 2(a) and the correspondence between in-plane vectors and index n in Table I]. Due to the C_3 symmetry of the lattice, the following equalities apply: $|t_3^{\alpha\beta}|=|t_1^{\alpha\beta}|$, $|t_5^{\alpha\beta}|=|t_4^{\alpha\beta}|$, and $|t_9^{\alpha\beta}|=|t_7^{\alpha\beta}|$. In addition, $t_1^{\alpha\beta}=t_2^{\alpha\beta}$ for $a_{1g} \rightarrow a_{1g}$ hoppings, which, however, does not hold for $e'_{g1,2}$ orbitals. Since the hybridization between the a_{1g} and the e'_g bands is not small, a simplified description of the bands crossing the Fermi level in terms of the a_{1g} band only [neglecting the e'_g band and the corresponding hybridizations (see, for example, Ref. 27)] may lead to an incorrect result due to a higher symmetry of the a_{1g} band.

In summary, the free-electron Hamiltonian for the CoO$_2$ plane in a hole representation is given by

$$H_0 = -\sum_{\mathbf{k},\alpha,\sigma} (\varepsilon^\alpha - \mu)n_{\mathbf{k}\alpha\sigma} - \sum_{\mathbf{k},\sigma} \sum_{\alpha,\beta} t_{\mathbf{k}}^{\alpha\beta} d_{\mathbf{k}\alpha\sigma}^\dagger d_{\mathbf{k}\beta\sigma}, \quad (1)$$

where $d_{\mathbf{k}\alpha\sigma}$ ($d_{\mathbf{k}\alpha\sigma}^\dagger$) is the annihilation (creation) operator for the hole with momentum $\mathbf{k}$, spin σ, and orbital index α, $n_{\mathbf{k}\alpha\sigma}=d_{\mathbf{k}\alpha\sigma}^\dagger d_{\mathbf{k}\alpha\sigma}$, and $t_{\mathbf{k}}^{\alpha\beta}$ is the Fourier transform of the hopping matrix element, ε^α is the single-electron energies, and μ is the chemical potential. Upon introducing matrix notations $(\hat{t}_{\mathbf{k}})_{\alpha\beta}=t_{\mathbf{k}}^{\alpha\beta}$ and $(\hat{t}_n)_{\alpha\beta}=t_n^{\alpha\beta}$, the hopping matrix elements in the momentum representation are given by

$$\hat{t}_{\mathbf{k}} = 2\hat{t}_1 \cos k_2 + 2\hat{t}_2 \cos k_3 + 2\hat{t}_3 \cos k_1 + 2\hat{t}_4 \cos(k_1+k_3)$$
$$+ 2\hat{t}_5 \cos(k_2+k_1) + 2\hat{t}_6 \cos(k_1-k_2) + 2\hat{t}_7 \cos 2k_2$$
$$+ 2\hat{t}_8 \cos 2k_3 + 2\hat{t}_9 \cos 2k_1, \quad (2)$$

where $k_1=(\sqrt{3}/2)k_x-\frac{1}{2}k_y$, $k_2=k_y$, and $k_3=(\sqrt{3}/2)k_x+\frac{1}{2}k_y$.

Note that the parameters do not change significantly upon changing the doping concentration. In Fig. 3, we show two results of the rigid-band approximation with the Hamiltonian [Eq. (1)] and the hopping values obtained through LDA calculation for two different doping concentrations, $x=0.33$ and
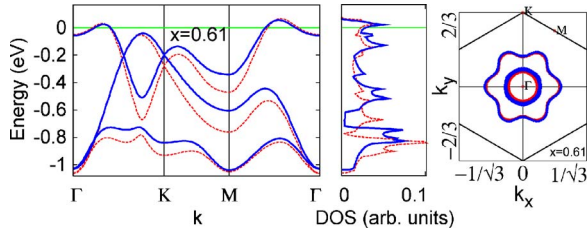
FIG. 3. (Color online) Calculated tight-binding energy dispersion, the density of states (DOS), and the Fermi surface for $Na_{0.61}CoO_2$ within the rigid-band approximation with *ab initio* parameters for $x=0.61$ (the solid blue curve) and for $x=0.33$ (red dashed curve). The horizontal (green) line denotes the chemical potential μ for $x=0.61$.

$x=0.61$ (see Table I). The doping concentration used to calculate the chemical potential μ was fixed to be $x=0.61$ for both Hamiltonians. Although one finds the pronounced differences in the dispersion around the M point, they are small around the FS. Since most of the physical quantities are determined by the states lying close to the Fermi level, we can safely ignore the small differences of the band structure and describe the doping evolution of the Na_xCoO_2 by simply varying the chemical potential. In the following, we will use *ab initio* parameters calculated for $x=0.33$ and change the chemical potential to achieve different doping concentrations.

Within the rigid-band approximation, the e_g' hole pockets are well below the Fermi level for $x \geqslant 0.41$. Most important, however, we find that the local minimum of the band dispersion around the Γ point (see Fig. 3) yields an inner FS contour centered around this point. The area of this electron FS pocket increases upon increasing the doping concentration x. As we will show later, the main reason for the local minimum around the Γ point is the presence of the next-nearest-neighbor hopping integrals, which enter our tight-binding dispersion. Although this minimum is not yet directly observed by ARPES experiments, note that the inner FS contour would reduce the total FS volume and therefore may explain why the volume of the FS observed in ARPES so far is larger than what follows from Luttinger's theorem.[28] Furthermore, an emergence of this pocket would influence the Hall conductivity at high doping concentrations, which would be interesting to check experimentally.

Note that the appearance of the inner contour of the FS around the Γ point for large doping concentrations is not unique to our calculations, previously, it has been obtained within the LDA calculations for a single Co layer per unit cell.[14]

III. MAGNETIC SUSCEPTIBILITY

To analyze the possibility of the itinerant magnetism, we calculate the magnetic susceptibility $\chi_0(\mathbf{q}, \omega=0)$ based on the Hamiltonian H_0. The doping-dependent evolution of the peaks in Re $\chi_0(\mathbf{q}, 0)$ is shown in Fig. 4. At $x=0.41$, the e_g' bands are below the Fermi level, and the FS takes the form of the rounded hexagon. This results in a number of nesting wave vectors around the antiferromagnetic wave vector
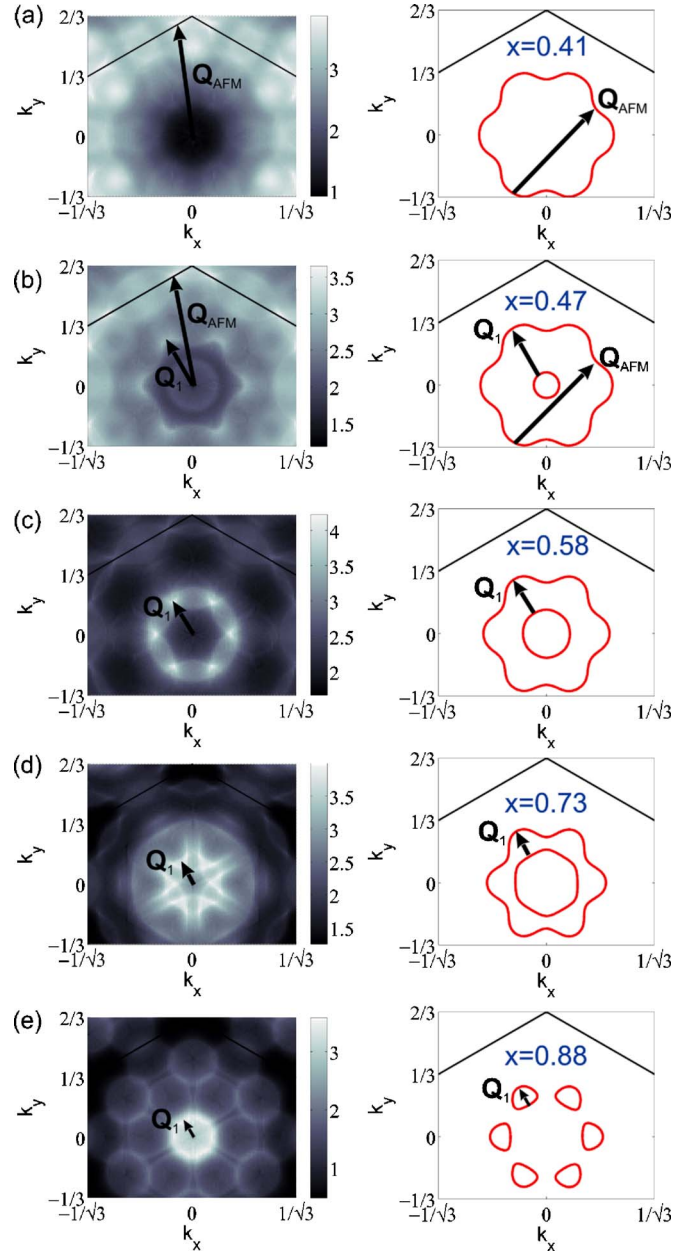

FIG. 4. (Color online) The contour plot of the real part of the magnetic susceptibility Re $\chi_0(\mathbf{k}, \omega=0)$ as a function of the momentum in units of $2\pi/a$ (left), and the Fermi surface for corresponding doping concentration x (right). The arrows indicate the scattering wave vectors $\mathbf{Q}_i$ as described in the text.

$\mathbf{Q}_{AFM}$. The corresponding broad peaks in the Re $\chi_0(\mathbf{q}, 0)$ appear around $\mathbf{Q}_{AFM}$, indicating the tendency of the electronic system toward a 120° AFM spin-density wave (SDW) ordered state.[29] Upon increasing doping, the Fermi level crosses the local minimum at the Γ point, resulting in an almost circular inner FS contour. As soon as this change of the FS topology occurs, the scattering at the momentum Q_{AFM} is strongly suppressed at $x_m \gtrsim 0.56$. Simultaneously, a new scattering vector $\mathbf{Q}_1$ at small momenta appears. Correspondingly, the magnetic susceptibility peaks at small momenta, indicating the tendency of the magnetic system toward an itinerant SDW order with small momenta. The
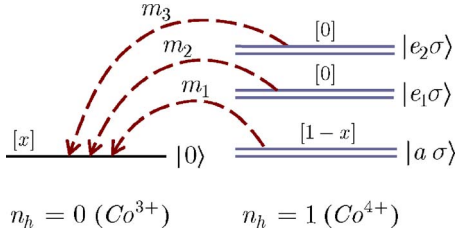
$$n_h = 0 \; (Co^{3+}) \qquad n_h = 1 \; (Co^{4+})$$

FIG. 5. (Color online) A schematic picture of the local atomic states on Co and the single-particle excitations in Na_xCoO_2. Here, n_h stands for number of holes and m_i enumerates single-particle excitations. The filling factor of the corresponding state upon changing the doping concentration x is given in square brackets.

relevance of the local minimum around the Γ point for the formation of the scattering at small momenta was originally found in Ref. 27.

For large x, the area of the inner FS contour increases, leading to a further decrease of the $\mathbf{Q}_1$. Observe that for $x \approx 0.88$, the FS topology again changes, yielding six distant FS contours that move $\mathbf{Q}_1$ further to zero momenta. The scattering at small momenta seen in the bare magnetic susceptibility for $x > x_m$ is qualitatively consistent with the ferromagnetic ordering at $\mathbf{Q}_{FM} = (0,0)$, observed in the neutron-scattering experiments.[18–20]

IV. EFFECTS OF STRONG ELECTRON CORRELATIONS

It is important to understand the impact of electronic correlations on the magnetic instabilities obtained within the rigid-band approximation. Since obtained magnetic susceptibility depends mostly on the topology of the FS one expects that the behavior shown in Fig. 4 will be valid even if one considers a random-phase approximation (RPA) susceptibility with an interaction term H_{int} taken into account, at least in case the only interaction is the on-site Hubbard repulsion U. The only difference would be a shift of the critical concentrations x_m, at which the FS topology changes and the tendency to the AFM order changes toward the tendency to the FM ordered state. Similar to Refs. 16 and 30, we add the on-site Coulomb interaction terms to Eq. (1). At present, it is not completely clear to which extent the electronic correlations govern the low-energy properties in Na_xCoO_2 due to multiorbital effects in this compound, which complicates the situation. Therefore, in the following, we discuss three different approximations valid for different U/t ratios.

A. Hubbard-I approximation

To analyze the regime of strong electron correlations, we project the doubly occupied states out and formulate an effective model equivalent to the Hubbard model with an infinite value of U. This approximation could be justified by the large ratio of the on-site Coulomb interaction on the CoO_2 cluster U with respect to the bandwidth W. In the atomic limit, the local low-energy states on the Co sites are the vacuum state $|0\rangle$ and the single-occupied hole states $|a\sigma\rangle$, $|e_1\sigma\rangle$, and $|e_2\sigma\rangle$. The single-particle hole excitations and local atomic states are shown in Fig. 5. The simplest way to

describe the quasiparticle excitations between these states is to use the projective Hubbard X operators that take the no-double occupancy constraint into account automatically:[31] $X_f^m \leftrightarrow X_f^{p,q} \equiv |p\rangle\langle q|$, where index $m \leftrightarrow (p,q)$ enumerates quasiparticles. There is a simple correspondence between the fermioniclike X operators and single-electron creation-annihilation operators: $d_{f\alpha\sigma} = \sum_m \gamma_{\alpha\sigma}(m) X_f^m$, where $\gamma_{\alpha\sigma}(m)$ determines the partial weight of a quasiparticle m with spin σ and orbital index α. In these notations, the Hamiltonian of the Hubbard model in the limit $U \to \infty$ has the form

$$H = -\sum_{f,p} (\varepsilon^p - \mu) X_f^{p,p} - \sum_{f \neq g} \sum_{m,m'} t_{fg}^{mm'} X_f^{m\dagger} X_g^{m'}. \quad (3)$$

To study a quasiparticle energy spectrum of the system and its thermodynamics, we use the Fourier transform of the two-time retarded Green function in the frequency representation $G_{\alpha\sigma}(\mathbf{k},E) \equiv \langle\langle d_{\mathbf{k}\alpha\sigma} | d_{\mathbf{k}\alpha\sigma}^\dagger \rangle\rangle_E$. This can be rewritten as $G_{\alpha\sigma}(\mathbf{k},E) = \sum_{m,m'} \gamma_{\alpha\sigma}(m) \gamma_{\beta\sigma}^*(m') D^{mm'}(\mathbf{k},E)$, where $D^{mm'}(\mathbf{k},E) = \langle\langle X_{\mathbf{k}}^m | X_{\mathbf{k}}^{m'\dagger} \rangle\rangle_E$ is the matrix Green function in the X-operator representation.

Using the diagram technique for Hubbard X operators,[32,33] one obtains the generalized Dyson equation[34]

$$\hat{D}(\mathbf{k},E) = [\hat{G}_0^{-1}(E) - \hat{P}(\mathbf{k},E)\hat{t}_{\mathbf{k}} + \hat{\Sigma}(\mathbf{k},E)]^{-1} \hat{P}(\mathbf{k},E). \quad (4)$$

Here, $\hat{G}_0^{-1}(E)$ stands for the (exact) local Green function, $G_0^{mm'}(E) = \delta_{mm'}/[E - (\varepsilon_p - \varepsilon_q)]$. In the Hubbard-I approximation, the self-energy $\hat{\Sigma}(\mathbf{k},E)$ is equal to zero and the strength operator $\hat{P}(\mathbf{k},E)$ is replaced by the sum of the occupation factors, $P^{mm'}(\mathbf{k},E) \to P^{mm'} = \delta_{mm'}(\langle X_f^{p,p} \rangle + \langle X_f^{q,q} \rangle)$, $m = m(p,q)$. Here, "$\langle \cdots \rangle$" stands for the usual thermodynamic average. Thus, one obtains

$$\hat{D}^{(0)}(\mathbf{k},E) = (\hat{G}_0^{-1} - \hat{P}\hat{t}_{\mathbf{k}})^{-1} \hat{P}. \quad (5)$$

In the paramagnetic phase, the occupation factors are $\langle X_f^{0,0} \rangle = x$, $\langle X_f^{a\sigma,a\sigma} \rangle = (1-x)/2$, $\langle X_f^{e1,2\sigma,e1,2\sigma} \rangle = 0$ which yields the diagonal form of the strength operator, and $\hat{P} = \text{diag}[(1+x)/2, x, x]$. Therefore, the quasiparticle bands formed by the $a_{1g} \to a_{1g}$ hoppings will be renormalized by the $(1+x)/2$ factor, while the quasiparticle bands formed by the e_g' hopping elements will be renormalized by x.

In Fig. 6, the quasiparticle spectrum, the DOS, and the FS are displayed in different approximations. Within Hubbard-I approximations, one finds the narrowing of the bands upon lowering the doping concentration x due to the doping dependence of the quasiparticle's spectral weight introduced by the strength operator $\hat{P}$. However, the doping evolution of the FS is qualitatively similar to that in the rigid-band picture. Namely, the bandwidth reduction and the spectral weight renormalization do not change the topology of the FS. As a result, the presence of the strong electronic correlations within Hubbard-I approximations does not qualitatively change our results for the bare susceptibility. Quantitatively, the critical concentration x_m shifts toward higher values of the doping and becomes $x_m \approx 0.68$. The reason for this shift is the band narrowing and the renormalization of
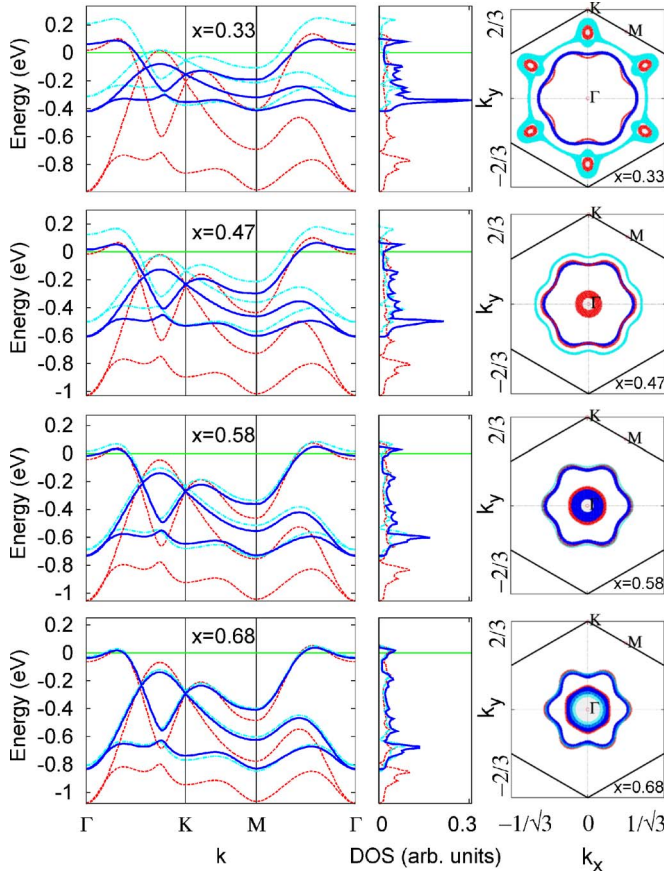
FIG. 6. (Color online) Calculated band structure and the Fermi surface topology for Na$_x$CoO$_2$ for $x=0.33$, 0.47, 0.58, and 0.68 The dashed (red), solid (blue), and dash-dotted (cyan) curves represent the results of the rigid-band, the Gutzwiller, and the Hubbard-I approximations, respectively. The horizontal (green) line denotes the position of the chemical potential μ.

the quasiparticle's spectral weight, which enters the equation that determines the position of the chemical potential μ.

Luttinger's theorem, which holds for a perturbative expansion of Green's function in terms of the interaction strength, is violated within the Hubbard-I approximation. This violation is due to the renormalization of the spectral weight of Green's function by the occupation factors in the strength operator in Eq. (4). This is the reason why in spite of the e'_g band narrowing, the e'_g hole pockets at the Fermi surface are still present at $x=0.33$.

B. Gutzwiller approximation

The Gutzwiller approximation[35–37] for the Hubbard model provides a good description for the correlated metallic system. Its multiband generalization was formulated in Ref. 38. In this approach, the Hamiltonian describing the interacting system far from the metal-insulator transition for $U \gg W$,

$$H = H_0 + \sum_{f,\alpha} U_\alpha n_{f\alpha\uparrow} n_{f\alpha\downarrow}, \tag{6}$$

with H_0 being the free electron Hamiltonian (1), is replaced by the effective noninteracting Hamiltonian

$$H_{\mathrm{eff}} = -\sum_{f,\alpha,\sigma} (\varepsilon^\alpha + \delta\varepsilon^{\alpha\sigma} - \mu) n_{f\alpha\sigma} - \sum_{f\neq g,\sigma} \sum_{\alpha,\beta} \tilde{t}^{\alpha\beta}_{fg} d^\dagger_{f\alpha\sigma} d_{g\beta\sigma} + C. \tag{7}$$

Here, $\tilde{t}^{\alpha\beta}_{fg} = t^{\alpha\beta}_{fg} \sqrt{q_{\alpha\sigma}} \sqrt{q_{\beta\sigma}}$ is the renormalized hopping, $q_{\alpha\sigma} = x/(1-n_{\alpha\sigma})$, $n_{\alpha\sigma} = \langle\Psi_0|n_{f\alpha\sigma}|\Psi_0\rangle \equiv \langle n_{f\alpha\sigma}\rangle_0$ is the orbital's filling factors, and $x = 1 - \sum_{\alpha\sigma} n_{\alpha\sigma}$ is the equation for the chemical potential. $\delta\varepsilon^{\alpha\sigma}$ are the Lagrange multipliers yielding the correlation-induced shifts of the single-electron energies. The constant C is determined from the condition that the ground-state energy is the same for both Hamiltonians,

$$\langle\Psi_0|H_{\mathrm{eff}}|\Psi_0\rangle = \langle\Psi_g|H|\Psi_g\rangle, \tag{8}$$

where $|\Psi_0\rangle$ is the wave function of the free-electron system [Eq. (7)] and $|\Psi_g\rangle$ is the Gutzwiller wave function for the Hamiltonian [Eq. (6)].

The Lagrange multipliers are determined by minimizing the energy,

$$\langle\Psi_0|H_{\mathrm{eff}}|\Psi_0\rangle = -\sum_{\alpha,\sigma} (\varepsilon^\alpha + \delta\varepsilon^{\alpha\sigma} - \mu)\langle n_{f\alpha\sigma}\rangle_0$$
$$- \sum_{f\neq g,\sigma} \sum_{\alpha,\beta} \tilde{t}^{\alpha\beta}_{fg} \langle d^\dagger_{f\alpha\sigma} d_{g\beta\sigma}\rangle_0 + C, \tag{9}$$

with respect to the orbital filling factors $n_{\alpha\sigma}$. Here, $C = \sum_{\alpha,\sigma} \delta\varepsilon^{\alpha\sigma} n_{\alpha\sigma}$, as determined from Eq. (8). This results in the following expression for the single-electron energy renormalizations:

$$\delta\varepsilon^{\alpha\sigma} = \frac{1}{2(1-n_{\alpha\sigma})} \sum_{f\neq g,\beta} \tilde{t}^{\alpha\beta}_{fg} \langle d^\dagger_{f\alpha\sigma} d_{g\beta\sigma}\rangle_0. \tag{10}$$

It is this energy shift that forces the e'_g FS hole pockets to sink below the Fermi energy,[16] which is clearly seen in the doping-dependent evolution of the quasiparticle dispersion and the FS, as obtained within the Gutzwiller approximation (Fig. 6). Although the narrowing of the bands due to strong correlations is similar to the one found in the Hubbard-I approximation, the FS obeys Luttinger's theorem. Note that, in contrast to the Hubbard-I approximation, the relative positions of the t_{2g} bands are also renormalized by $\delta\varepsilon^{\alpha\sigma}$.

At the same time, for $x > 0.4$, the topology of the FS in the Gutzwiller approximation is qualitatively the same as in the rigid-band picture. This also yields similar results for the bare susceptibility's doping dependence discussed in Sec. III. The only effect of the strong correlations for χ_0 is the observed shift of the critical concentration toward higher values, $x_m \approx 0.6$. This is due to combined effect of the bands narrowing and the doping dependence of the a_{1g} and e'_g bands' relative positions, determined by Eq. (10).

Note that, for $x < 0.4$, due to different FS topologies that occur in the Gutzwiller approximation, the bare susceptibility differs from that obtained in Ref. 29 where the strong renormalization of the electronic bands removing e'_g pockets from the FS was neglected.

C. Fluctuation exchange approximation

A certain disadvantage of the Gutzwiller- and Hubbard-I-like approximations is that the dynamic character of elec-

tronic correlations is not taken into account within these approaches. At the same time, the momentum and frequency dependencies of the self-energy $\Sigma(\mathbf{k}, \omega)$ play a crucial role, in particular, in determining the low-energy excitations close to the Fermi level. In this section, we focus on the a_{1g} band with nearest- and next-nearest-neighbor hopping integrals only and employ the single-band FLEX (Ref. 39) approximation which sums all particle-hole (particle) ladder graphs for the generating functional self-consistently valid for intermediate strength of the correlations. The FLEX equations for the single-particle Green's function G, the self-energy Σ, the effective interaction V, the bare (χ^0), and renormalized spin (χ^s) and charge (χ^c) susceptibilities read

$$G_{\mathbf{k}}(\omega_n) = [\omega_n - \tau_{\mathbf{k}} + \mu - \Sigma_{\mathbf{k}}(\omega_n)]^{-1}, \qquad (11)$$

$$\Sigma_{\mathbf{k}}(\omega_n) = \frac{T}{N}\sum_{\mathbf{p},m} V_{\mathbf{k}-\mathbf{p}}(\omega_n - \omega_m)G_{\mathbf{p}}(\omega_m), \qquad (12)$$

$$V_{\mathbf{q}}(\nu_m) = U^2\left[\frac{3}{2}\chi_{\mathbf{q}}^s(\nu_m) + \frac{1}{2}\chi_{\mathbf{q}}^c(\nu_m) - \chi_{\mathbf{q}}^0(\nu_m)\right], \qquad (13)$$

$$\chi_{\mathbf{q}}^0(\nu_m) = -\frac{T}{N}\sum_{\mathbf{k},n} G_{\mathbf{k}+\mathbf{q}}(\omega_n + \nu_m)G_{\mathbf{k}}(\omega_n), \qquad (14)$$

$$\chi_{\mathbf{q}}^{s,c}(\nu_m) = \frac{\chi_{\mathbf{q}}^0(\nu_m)}{1 \mp U\chi_{\mathbf{q}}^0(\nu_m)}, \qquad (15)$$

where $\omega_n = i\pi T(2n+1)$ and $\nu_m = i\pi T(2m)$. Here $\tau_{\mathbf{k}}$ is the a_{1g} bare band dispersion. In the last equation, the "$-$" sign in the denominator corresponds to the $\chi_{\mathbf{q}}^s(\nu_m)$, while the "$+$" sign corresponds to the $\chi_{\mathbf{q}}^c(\nu_m)$. We compute the Matsubara summations using the "almost real contour" technique of Ref. 40. That is, the contour integrals are performed with a finite shift $i\gamma$ ($0 < \gamma < iT\pi/2$) into the upper half-plane. All final results are analytically continued from $\omega + i\gamma$ onto the real axis $\omega + i0^+$ by Padé approximation. The following results are based on FLEX solutions using a lattice of 64×64 sites with 4096 equidistant ω points in the energy range of $[-30, 30]$. The temperature has been kept at $T = 0.05\tau$, where τ is the hopping amplitude to the nearest neighbors for the a_{1g} band corresponding to $t_1^{a_{1g}a_{1g}} = t_2^{a_{1g}a_{1g}} = t_3^{a_{1g}a_{1g}}$. The Hubbard repulsion was set to $U = 8\tau$.

Previously, the FLEX approximation has been applied successfully to the study of superconductivity as well as spin and charge excitations in Na_xCoO_2.[41,42] Complementary to this, we will focus on the quasiparticle dispersion and study the impact of the momentum and frequency dependencies of the $\Sigma(\mathbf{k}, \omega)$, and the role played by the next-nearest-neighbor hopping integral τ' corresponding to $t_4^{a_{1g}a_{1g}} = t_5^{a_{1g}a_{1g}} = t_6^{a_{1g}a_{1g}}$. The quasiparticle dispersion $E_{\mathbf{k}}$, which is determined from equation $E_{\mathbf{k}} - \tau_{\mathbf{k}} + \mu - \Sigma_{\mathbf{k}}(E_{\mathbf{k}}) = 0$, is shown in Fig. 7 for $\tau' = 0$ and $\tau' = -0.45$, in units of τ. First, observe that the local minimum around the Γ point appears only if the next-nearest-neighbor hopping integral τ' is included which agrees with our previous findings. In addition, we obtain a pronounced mass enhancement of the order of unity at the FS crossings—the so-called kink structure. This enhance-
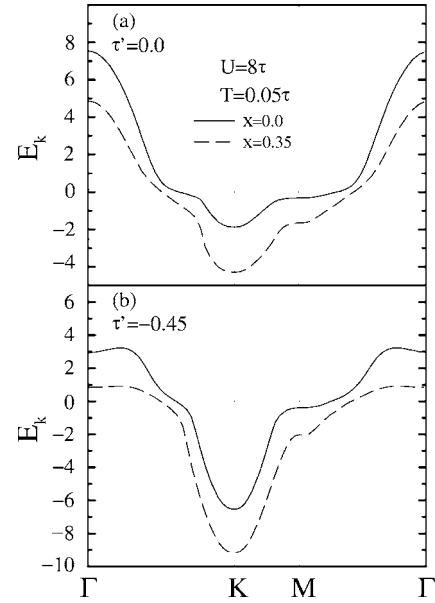

FIG. 7. Quasiparticle dispersion $E_{\mathbf{k}}$ (in units of τ, relative to μ) within FLEX approximation for (a) $\tau' = 0$ and (b) $\tau' = -0.45$ and for two doping concentrations.

ment is due to low-energy spin fluctuations which are present in $\chi_{\mathbf{q}}^s(\omega)$.[41]

To shed more light on the two-dimensional spin correlations, in Fig. 8 we display the static spin structure factor Re $\chi_{\mathbf{k}}^s(\omega=0)$ from the FLEX for two different doping concentrations. As doping increases from $x=0$ toward $x=0.35$, the maximum in the spin susceptibility $\chi_{\mathbf{k}}^s(\omega=0)$ moves toward the K point of the first Brillouin zone (BZ) and develops into a sharp and commensurate peak at $\mathbf{Q}_{AFM}$, and the incommensurate spin fluctuations are suppressed. One may also note that the commensurate peak is $\sim 60\%$ larger for
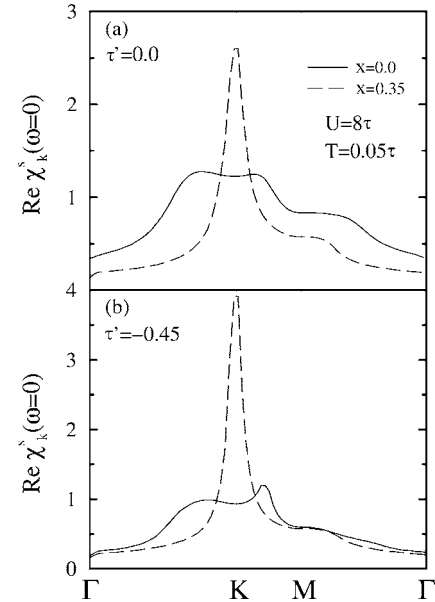

FIG. 8. Doping dependence of the static spin structure factor Re $\chi_{\mathbf{k}}^s(\omega=0)$ for (a) $\tau' = 0$ and (b) $\tau' = -0.45$. Note that for large $U = 8\tau$, the commensurate peak at K point is absent at a very low x.
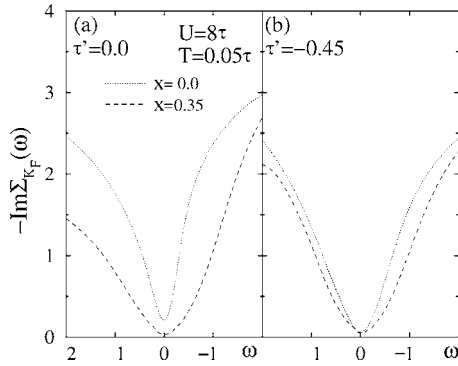
FIG. 9. Frequency dependence of quasiparticle self-energy $-\text{Im}\,\Sigma_\mathbf{k}$ near the FS in direction Γ-K for (a) $\tau'=0$ and (b) $\tau'=-0.45$.

$\tau'=-0.45$ than for $\tau'=0$. These results are consistent with those obtained in previous sections. We further notice that the quasiparticle dynamics go through a smooth evolution with doping in Na$_x$CoO$_2$, and show no signs of unusual behavior at $x=0$.

The frequency dependence of the imaginary part of the quasiparticle self-energy, i.e., Im $\Sigma_\mathbf{k}$, near the FS is shown in Fig. 9. We find the self-energy to be nearly isotropic along the FS with only a weak maximum occurring into the direction of the commensurate spin fluctuations. Near the Fermi energy, the self-energy is clearly proportional to ω^2 at low energies for all dopings shown, which is indicative of the normal Fermi-liquid behavior. This is in sharp contrast to the FLEX analysis of the Hubbard model on the square lattice close to a half-filling. There one typically finds "marginal" Fermi-liquid behavior with Im $\Sigma_\mathbf{k} \approx \omega$ over a wide range of frequencies.[43,44] Therefore, along this line one is tempted to conclude that the normal state of the superconducting cobaltates is more of a conventional metallic nature than in the high-T_c cuprates. This becomes even more evident, if one realizes from Fig. 9 that the quasiparticle scattering rate displays its smallest curvature for $x=0.35$, which implies that the quasiparticles are rather well defined there. For lower x, the proximity of the FS to the van Hove singularity (see flat region of dispersion in Fig. 7) enhances both the absolute value of Im $\Sigma_\mathbf{k} \propto \omega$ and of the curvature. This effect is most pronounced for $\tau'=0$.

V. CONCLUSION

To conclude, we have calculated the doping-dependent magnetic susceptibility in the tight-binding model with *ab initio* calculated parameters and found that, at a critical doping concentration x_m, electron pocket develops on the FS in the center of the Brillouin zone. For $x<x_m$, the system shows a tendency toward a 120° AFM ordered state, while for $x>x_m$, a peak in the magnetic susceptibility forms at small wave vectors, indicating a strong tendency toward an itinerant FS state. Within a tight-binding model, we have estimated x_m to be approximately 0.56. Analyzing the influence of a strong Coulomb repulsion and the corresponding reduction of the bandwidth and the quasiparticle spectral weight in the strong-coupling Hubbard-I and Gutzwiller approximations, we have shown that the critical concentration changes to $x_m \approx 0.68$ and $x_m \approx 0.6$, respectively. At the same time, the underlying physics of the formation of the itinerant FM state remains the same.

We neglected the bonding-antibonding splitting due to the three dimensionality in the nonintercalated compounds. This splitting was taken into account in Ref. 41, where within the FLEX approximation, the single a_{1g}-band Hubbard model was considered. The results obtained also suggest a tendency to FM fluctuations for high doping concentrations. The presence of a local band minimum around the Γ point played a crucial role, as we also found in our present study.

To analyze the low-energy quasiparticle properties at low doping concentrations, we have employed the single-band Hubbard model within the FLEX approximation. We have found a significant FS mass enhancement of order unity due to quasiparticle scattering from spin fluctuations. In contrast to the Hubbard model on the square lattice, we have found that the quasiparticle scattering rate displays a conventional Fermi-liquid type of energy dependence. We have also shown that the static spin structure factor exhibits a large commensurate peak at wave vector $\mathbf{Q}_{\text{AFM}}$ for doping concentrations of $x\approx0.35$. This response was found to be significantly enhanced by the next-nearest-neighbor hopping, emphasizing its significance.

*Electronic address: maxim@mpipks-dresden.mpg.de
[1] K. Takada, H. Sakurai, E. Takayama-Muromachi, F. Izumi, R. A. Dilanian, and T. Sasaki, Nature (London) **422**, 53 (2003).
[2] I. Terasaki, Y. Sasago, and K. Uchinokura, Phys. Rev. B **56**, R12685 (1997).
[3] Y. Wang, N. Rogado, R. J. Cava, and N. P. Ong, Nature (London) **423**, 425 (2003).
[4] M. L. Foo, Y. Wang, S. Watauchi, H. W. Zandbergen, T. He, R. J. Cava, and N. P. Ong, Phys. Rev. Lett. **92**, 247001 (2004).
[5] B. C. Sales, R. Jin, K. A. Affholter, P. Khalifah, G. M. Veith, and D. Mandrus, Phys. Rev. B **70**, 174419 (2004).
[6] D. J. Singh, Phys. Rev. B **61**, 13397 (2000).

[7] K.-W. Lee, J. Kuneš, and W. E. Pickett, Phys. Rev. B **70**, 045104 (2004).

[8] M. Z. Hasan, Y.-D. Chuang, D. Qian, Y. W. Li, Y. Kong, A. Kuprin, A. V. Fedorov, R. Kimmerling, E. Rotenberg, K. Rossnagel, Z. Hussain, H. Koh, N. S. Rogado, M. L. Foo, and R. J. Cava, Phys. Rev. Lett. **92**, 246402 (2004).

[9] H.-B. Yang, S.-C. Wang, A. K. P. Sekharan, H. Matsui, S. Souma, T. Sato, T. Takahashi, T. Takeuchi, J. C. Campuzano, R. Jin, B. C. Sales, D. Mandrus, Z. Wang, and H. Ding, Phys. Rev. Lett. **92**, 246403 (2004).

[10] H.-B. Yang, Z.-H. Pan, A. K. P. Sekharan, T. Sato, S. Souma, T. Takahashi, R. Jin, B. C. Sales, D. Mandrus, A. V. Fedorov, Z. Wang, and H. Ding, Phys. Rev. Lett. **95**, 146401 (2005).

[11] D. Qian, D. Hsieh, L. Wray, Y.-D. Chuang, A. Fedorov, D. Wu, J. L. Luo, N. L. Wang, L. Viciu, R. J. Cava, and M. Z. Hasan, Phys. Rev. Lett. **96**, 216405 (2006).

[12] L. Balicas, J. G. Analytis, Y. J. Jo, K. Storr, H. Zandbergen, Y. Xin, N. E. Hussey, F. C. Chou, and P. A. Lee, Phys. Rev. Lett. **97**, 126401 (2006).

[13] D. J. Singh and D. Kasinathan, Phys. Rev. Lett. **97**, 016404 (2006).

[14] P. Zhang, W. Luo, M. L. Cohen, and S. G. Louie, Phys. Rev. Lett. **93**, 236402 (2004).

[15] H. Ishida, M. D. Johannes, and A. Liebsch, Phys. Rev. Lett. **94**, 196401 (2005).

[16] S. Zhou, M. Gao, H. Ding, P. A. Lee, and Z. Wang, Phys. Rev. Lett. **94**, 206401 (2005).

[17] D. J. Singh, Phys. Rev. B **68**, 020503(R) (2003).

[18] A. T. Boothroyd, R. Coldea, D. A. Tennant, D. Prabhakaran, L. M. Helme, and C. D. Frost, Phys. Rev. Lett. **92**, 197201 (2004).

[19] S. P. Bayrakci, I. Mirebeau, P. Bourges, Y. Sidis, M. Enderle, J. Mesot, D. P. Chen, C. T. Lin, and B. Keimer, Phys. Rev. Lett. **94**, 157205 (2005).

[20] L. M. Helme, A. T. Boothroyd, R. Coldea, D. Prabhakaran, D. A. Tennant, A. Hiess, and J. Kulda, Phys. Rev. Lett. **94**, 157206 (2005).

[21] W. Kohn and L. J. Sham, Phys. Rev. A **140**, 1133 (1965).

[22] O. K. Andersen and O. Jepsen, Phys. Rev. Lett. **53**, 2571 (1984).

[23] J. D. Jorgensen, M. Avdeev, D. G. Hinks, J. C. Burley, and S. Short, Phys. Rev. B **68**, 214517 (2003).

[24] N. Marzari and D. Vanderbilt, Phys. Rev. B **56**, 12847 (1997).

[25] V. I. Anisimov, D. E. Kondakov, A. V. Kozhevnikov, I. A. Nekrasov, Z. V. Pchelkina, J. W. Allen, S.-K. Mo, H.-D. Kim, P. Metcalf, S. Suga, A. Sekiyama, G. Keller, I. Leonov, X. Ren, and D. Vollhardt, Phys. Rev. B **71**, 125119 (2005).

[26] M. D. Johannes, D. A. Papaconstantopoulos, D. J. Singh, and M. J. Mehl, Europhys. Lett. **68**, 433 (2004).

[27] K. Kuroki, S. Onari, Y. Tanaka, R. Arita, and T. Nojima, Phys. Rev. B **73**, 184503 (2006).

[28] S. Borisenko (private communication).

[29] M. D. Johannes, I. I. Mazin, D. J. Singh, and D. A. Papaconstantopoulos, Phys. Rev. Lett. **93**, 097005 (2004).

[30] M. Indergand, Y. Yamashita, H. Kusunose, and M. Sigrist, Phys. Rev. B **71**, 214414 (2005).

[31] J. C. Hubbard, Proc. R. Soc. London, Ser. A **277**, 237 (1964).

[32] R. O. Zaitsev, Sov. Phys. JETP **41**, 100 (1975).

[33] Yu. Izumov and B. M. Letfullov, J. Phys.: Condens. Matter **3**, 5373 (1991).

[34] S. G. Ovchinnikov and V. V. Val'kov, *Hubbard Operators in the Theory of Strongly Correlated Electrons* (Imperial College Press, London, 2004).

[35] M. C. Gutzwiller, Phys. Rev. Lett. **10**, 159 (1963); Phys. Rev. **134**, A923 (1964); Phys. Rev. **A137**, 1726 (1965).

[36] F. Gebhard, Phys. Rev. B **41**, 9452 (1990).

[37] G. Kotliar and A. E. Ruckenstein, Phys. Rev. Lett. **57**, 1362 (1986).

[38] J. Bünemann, F. Gebhard, and W. Weber, J. Phys.: Condens. Matter **9**, 7343 (1997).

[39] N. E. Bickers, D. J. Scalapino, and S. R. White, Phys. Rev. Lett. **62**, 961 (1989); J. Altmann, W. Brenig, and A. P. Kampf, Eur. Phys. J. B **18**, 429 (2000).

[40] J. Schmalian, M. Langer, S. Grabowski, and K. H. Bennemann, Comput. Phys. Commun. **93**, 141 (1996).

[41] K. Kuroki, S. Ohkubo, T. Nojima, R. Arita, S. Onari, and Y. Tanaka, cond-mat/0610494 (unpublished); K. Kuroki, S. Onari, Y. Tanaka, R. Arita, and T. Nojima, Phys. Rev. B **73**, 184503 (2006).

[42] Y. Yanase, M. Mochizuki, and M. Ogata, J. Phys. Soc. Jpn. **74**, 2568 (2005); **74**, 3351 (2005).

[43] J. Altmann, W. Brenig, and A. P. Kampf, Eur. Phys. J. B **18**, 429 (2000).

[44] S. Wermbter, Phys. Rev. B **55**, R10149 (1997).